Inorganic Chemistry

Article

pubs.acs.org/IC

Exchange Coupling and Its Chemical Trend Studied by High-Frequency EPR on Heterometallic [Ln_2Ni] Complexes

Atsushi Okazawa,[†] Takashi Shimada,[‡] Norimichi Kojima,[†] Shunsuke Yoshii,[§] Hiroyuki Nojiri,[§] and Takayuki Ishida*[,‡]

[†]Department of Basic Science, Graduate School of Arts and Sciences, The University of Tokyo, Meguro-ku, Tokyo 153-8902, Japan

[‡]Department of Engineering Science, The University of Electro-Communications, Chofu, Tokyo 182-8585, Japan

[§]Institute for Materials Research, Tohoku University, Katahira, Sendai 980-8577, Japan

Supporting Information

ABSTRACT: We applied high-frequency electron paramagnetic resonance to trinuclear 4f–3d heterometallic complexes, [{Ln(hfac)$_3$}$_2${Ni(dpk)$_2$(py)$_2$}] (Ln = Y, Gd, Tb, and Ho; hfac = hexafluoroacetylacetonate, dpk = di-2-pyridyl ketoximate, and py = pyridine), and determined the exchange parameter J_{Ln-Ni} as well as nickel(II) zero-field splitting parameters. In contrast to the antiferromagnetic Dy analogue, ferromagnetic couplings were precisely characterized as J_{Gd-Ni}/k_B = +0.301(4) K, J_{Tb-Ni}/k_B = +0.216(12) K, and J_{Ho-Ni}/k_B = +0.110(3) K (defined as $-J_{Ln-Ni}\sum J_{Ln}{}^{z}S_{Ni}$).

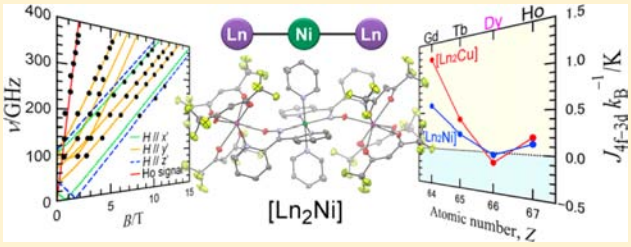

INTRODUCTION

Molecule-based magnetic materials have an advantage for chemists designing a spatial arrangement of various magnetic orbitals and preparing low-dimensional frameworks by means of facile self-assembly techniques.[1] Heterometallic 4f–3d coordination compounds have been intensively studied for investigating magneto–structure correlation since the first ferromagnetic Cu^{2+}–Gd^{3+} complexes were reported.[2] Recently, 4f–3d compounds have been developed toward single-molecule magnets,[3] where strong magnetic anisotropy and large spin are available from lanthanide (Ln) ions such as Tb^{3+}, Dy^{3+}, and Ho^{3+}.[4] In addition, isotropic Gd^{3+} has been more recently revived in developing molecular refrigerants with a large magnetocaloric effect.[5]

The exchange coupling constant (J_{Ln-M}) between 4f and 3d spins is one of the most important physical parameters, but there have scarcely been direct methods to evaluate it. Recently, we have established a standard method to determine quantitatively the exchange coupling[6] by means of combined high-frequency electron paramagnetic resonance (HF-EPR) and pulsed-field magnetization.[7] The J_{Ln-M} values were evaluated for various Ln^{III}–Cu^{II} and Ln^{III}–$V^{IV}O$ complexes.[6,8−11] Moreover, we found a Ln dependence of J_{Ln-M} values in these systems. The Cu and V ions are utilized as a probe for the exchange field because the g = 2 and $S = {}^1/_2$ signal can be easily traced in the EPR spectra. For further exploration of this method to various 3d metal ions with $S > {}^1/_2$, we moved on to study trinuclear Ln^{3+}–Ni^{2+} compounds, [{Ln(hfac)$_3$}$_2${Ni(dpk)$_2$(py)$_2$}] (abbreviated as [Ln_2Ni]; hfac = hexafluoroacetylacetonate, dpk = di-2-pyridyl ketoximate, and py = pyridine; Figure 1a). We have already reported a pilot experiment on [Dy_2Ni],[10a,b] but its systematic study is unprecedented and highly needed to comprehend the Ln–Ni physics and chemistry.

EXPERIMENTAL SECTION

Preparation. Complexes [{Ln(hfac)$_3$}$_2${Ni(dpk)$_2$(py)$_2$}] ([Ln_2Ni]; Ln = Y, Gd, Tb, and Ho) were synthesized according to the preparation method reported for [Dy_2Ni].[12] We also prepared Pd (S = 0; diamagnetic) analogues [{Ln(hfac)$_3$}$_2${Pd(dpk)$_2$}] ([Ln_2Pd]; Ln = Tb and Ho) for the reference samples on the $\Delta(\chi_{mol}T)$ versus T plots using a method similar to that of reported [Dy_2Pd].[13] For [Y_2Ni], Anal. Calcd for $C_{62}H_{32}F_{36}N_8NiO_{14}Y_2$: C, 36.62; H, 1.59; N, 5.51%. Found: C, 36.73; H, 1.51; N, 5.63%. IR (KBr disc) 1656, 1257, 1210, 1147, 662 cm^{-1}. Yield, 39%. For [Gd_2Ni], Anal. Calcd for $C_{62}H_{32}F_{36}N_8NiO_{14}Gd_2$: C, 34.31; H, 1.49; N, 5.16%. Found: C, 34.09; H, 1.18; N, 5.08%. IR (KBr disc) 1652, 1259, 1210, 1147, 662 cm^{-1}. Yield, 37%. For [Tb_2Ni], Anal. Calcd for $C_{62}H_{32}F_{36}N_8NiO_{14}Tb_2$: C, 34.26; H, 1.48; N, 5.16%. Found: C: 33.89, H: 1.24, N: 4.98%. IR (KBr disc) 1652, 1258, 1211, 1147, 662 cm^{-1}. Yield, 30%. For [Ho_2Ni], Anal. Calcd for $C_{62}H_{32}F_{36}N_8NiO_{14}Ho_2$: C, 34.07; H, 1.48; N, 5.13%. Found: C, 33.96; H, 1.61; N, 4.86%. IR (KBr disc) 1656, 1257, 1211, 1146, 662 cm^{-1}. Yield, 85%. For [Tb_2Pd], Anal. Calcd for $C_{52}H_{22}F_{36}N_6O_{14}PdTb_2$: C, 30.27; H, 1.07; N, 4.07%. Found: C: 30.04, H: 0.87, N: 3.96%. IR (KBr disc) 1652, 1258, 1210, 1147, 661 cm^{-1}. Yield, 64%. For [Ho_2Pd], Anal. Calcd for $C_{52}H_{22}F_{36}N_6O_{14}PdHo_2$: C, 30.10; H, 1.07; N, 4.05%. Found: C, 30.00; H, 0.85; N, 4.02%. IR (KBr disc) 1652, 1258, 1210, 1147, 662 cm^{-1}. Yield, 56%.

X-ray Crystallographic Studies. X-ray diffraction data of [Ln_2Ni] (Ln = Y, Gd, Tb, and Ho) were collected on a Rigaku R-axis RAPID IP or a Saturn70 CCD diffractometer with graphite monochromated Mo Kα radiation (λ = 0.71073 Å). The structures were directly solved

Received: June 7, 2013
Published: November 14, 2013

   dx.doi.org/10.1021/ic402417h | Inorg. Chem. 2013, 52, 13351−13355

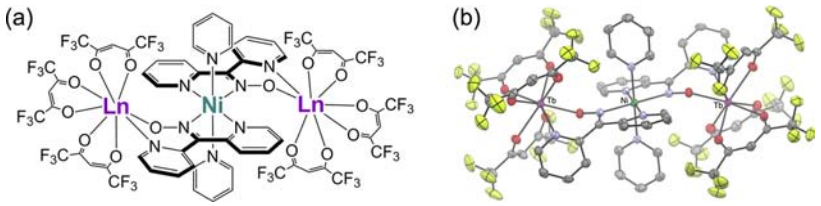

Figure 1. (a) General structural formula of $[Ln_2Ni]$ and (b) X-ray crystal structure of $[Tb_2Ni]$ with the thermal ellipsoids at the 50% probability level. Hydrogen atoms are omitted for clarity.

Table 1. Selected Crystallographic Data for $[Ln_2Ni]$ (Ln = Y, Gd, Tb, and Ho)

compounds	$[Y_2Ni]$	$[Gd_2Ni]$	$[Tb_2Ni]$	$[Ho_2Ni]$
formula	$C_{62}H_{32}F_{36}N_8NiO_{14}Y_2$	$C_{62}H_{32}F_{36}Gd_2N_8NiO_{14}$	$C_{62}H_{32}F_{36}N_8NiO_{14}Tb_2$	$C_{62}H_{32}F_{36}Ho_2N_8NiO_{14}$
formula weight	2033.4	2170.1	2173.4	2185.5
crystal system	monoclinic	monoclinic	monoclinic	monoclinic
space group	$P2_1/n$	$P2_1/n$	$P2_1/n$	$P2_1/n$
T, K	131	90	105	100
a, Å	10.8618(2)	10.851(6)	10.8639(2)	10.867(16)
b, Å	14.7511(3)	14.736(7)	14.7524(3)	14.769(19)
c, Å	23.5701(6)	23.50(3)	23.5802(6)	23.51(4)
β, deg	100.4394(6)	100.602(9)	100.6499(8)	100.51(13)
V, Å^3	3713.97(14)	3694(5)	3714.07(14)	3711(9)
Z	2	2	2	2
d_{calc}, g cm^{-3}	1.818	1.951	1.943	1.956
μ, mm^{-1}	1.960	2.190	2.288	2.523
λ, Å	0.71073	0.71073	0.71073	0.71073
R_{int}	0.1394	0.0842	0.0586	0.1173
R (F) $(I > 2\sigma(I))^a$	0.0512	0.0340	0.0342	0.0689
R_w (F^2) (all data)^b	0.0310	0.0456	0.0309	0.0871
GOF	1.038	0.979	1.030	1.154
unique reflections	8291	8273	8283	8174

$^aR = \Sigma||F_o| - ||F_c||/\Sigma|F_o|$. $^bR_w = [\Sigma w(F_o^2 - F_c^2)^2/\Sigma w(F_o^2)^2]^{1/2}$.

by a heavy-atom method and expanded using Fourier techniques in the CrystalStructure 4.0 program package (Rigaku, Tokyo, Japan). All of the hydrogen atoms were located at calculated positions, and the parameters were refined as riding. The thermal displacement parameters of non-hydrogen atoms were refined anisotropically. Full-matrix least-squares methods were applied using all of the unique reflection data. Selected crystallographic data are listed in Table 1.

Magnetic Measurements. The dc magnetic susceptibilities and low-temperature magnetization were recorded on a Quantum Design MPMS SQUID magnetometer. Polycrystalline samples (except for $[Gd_2Ni]$) were fixed in *n*-eicosane. The magnetic responses were corrected with the diamagnetic blank data of the sample holder measured separately. The diamagnetic contribution of the sample itself was estimated from Pascal's constant.

Pulsed-field magnetization was measured by a conventional inductive probe in pulsed-magnetic fields, and the temperature reached as low as 0.5 K using a ^{3}He cryostat.[7b] Polycrystalline specimens (typically 20 mg) were mounted in a capillary made of polyimide Kapton. The sample was not fixed within the sample tube and it was then aligned along the magnetic-field direction. After we applied the magnetic field several times, the orientation effect was saturated, and the magnetization curves obtained in further shots were found to be identical.

HF-EPR Measurements. HF-EPR spectra for polycrystalline samples were obtained by using a simple transmission method with a homemade HF-EPR spectrometer (TESRA-IMR).[7a] The sample was packed in a case made of polyethylene. The radiation was produced by Gunn oscillators and backward-traveling wave oscillators. The temperature was controlled using a ^{4}He cryostat.

RESULTS AND DISCUSSION

We prepared $[Ln_2Ni]$ (Ln = Y, Gd, Tb, and Ho) according to a known procedure[12] and successfully characterized them by single-crystal X-ray diffraction analyses (Figure 1a for Ln = Tb and Figure 1S (Supporting Information) for Ln = Y, Gd, and Ho). Selected bond lengths are summarized in Table 2. Their crystal structures are isomorphous to that of the known $[Dy_2Ni]$.[10a] The Ln^{3+} and Ni^{2+} ions are bridged with the O−N group of an oximate ligand. Each Ln ion forms an eight-coordinate square antiprism. The complexes have an inversion

Table 2. Selected Bond Lengths (Å) for $[Ln_2Ni]$ (Ln = Gd, Tb, Dy,[12] and Ho)

compounds	$[Gd_2Ni]$	$[Tb_2Ni]$	$[Dy_2Ni]$	$[Ho_2Ni]$
Ln1−O1	2.216(3)	2.230(2)	2.222(7)	2.225(7)
Ln1−O2	2.349(4)	2.361(3)	2.387(8)	2.357(8)
Ln1−O3	2.345(3)	2.362(3)	2.373(7)	2.330(7)
Ln1−O4	2.363(4)	2.377(3)	2.399(7)	2.357(7)
Ln1−O5	2.339(3)	2.362(3)	2.359(7)	2.353(7)
Ln1−O6	2.410(4)	2.417(3)	2.441(7)	2.413(7)
Ln1−O7	2.341(4)	2.359(2)	2.379(7)	2.338(8)
Ln1−N1	2.574(4)	2.588(3)	2.615(9)	2.584(8)
Ni1−N2	2.101(4)	2.101(3)	2.155(8)	2.106(8)
Ni1−N3	2.082(4)	2.080(3)	2.137(8)	2.088(7)
Ni1−N4	2.104(5)	2.098(3)	2.118(8)	2.115(8)
N3−O1	1.346(6)	1.331(4)	1.36(1)	1.33(1)

dx.doi.org/10.1021/ic402417h | *Inorg. Chem.* 2013, 52, 13351−13355

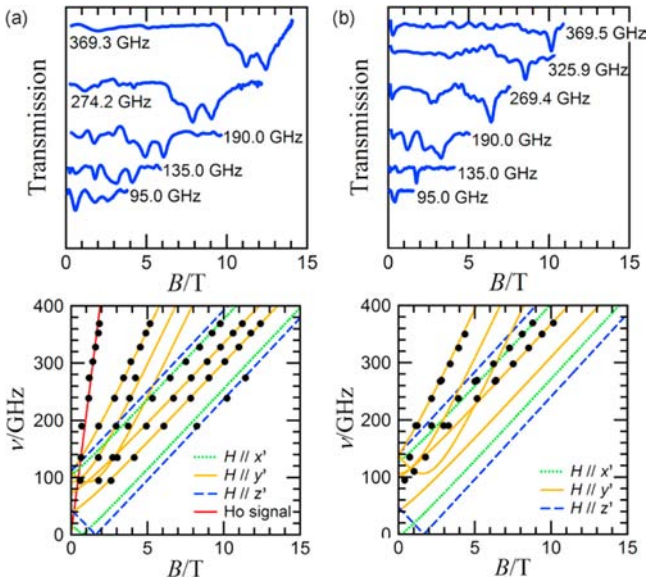

Figure 2. Top: selected EPR spectra measured at 4.2 K as a function of frequency for (a) [Ho_2Ni] and (b) [Tb_2Ni]. The spectra are offset on a linear scale of the frequency. Bottom: frequency-field diagrams. Lines stand for the best fit in eq 1 (see the text).

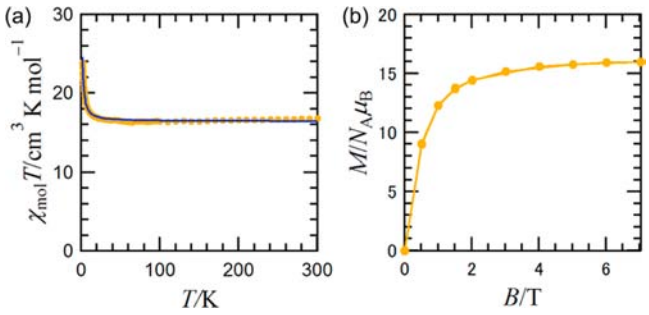

Figure 3. (a) Temperature dependence of $\chi_{mol}T$ for polycrystalline samples of [Gd_2Ni] at 500 Oe. The filled circles and solid line represent experimental data and the theoretical best fit, respectively, with g_{avg} = 1.968(3), J_{Gd-Ni}/k_B = +0.602(8) K, and χ_{TIP} = 1.3(3) × 10^{-5} cm^3 mol^{-1}. (b) Magnetization curve of a polycrystalline samples of [Gd_2Ni] at 1.8 K. A solid line is shown as a guide to the eye.

center at the Ni ion and thus there is a unique J_{Ln-Ni} exchange coupling.

Pulse-field magnetization measurements on field-oriented polycrystalline specimens were carried out for [Tb_2Ni] and [Ho_2Ni] (Figure S2). No magnetization step was observed, suggesting that J_{Tb-Ni} and J_{Ho-Ni} are ferromagnetic. The saturated magnetizations (M_S) of [Tb_2Ni] and [Ho_2Ni] were

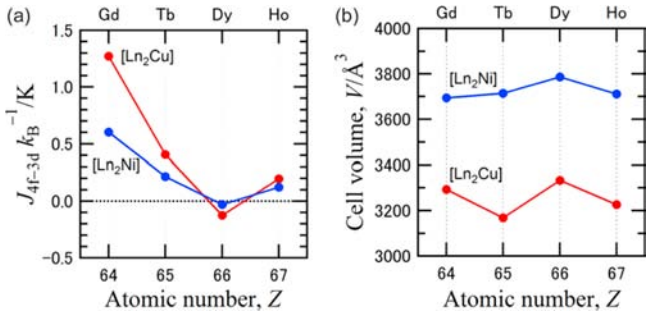

Figure 5. (a) Plot of the 4f–3d exchange parameters in [Ln_2Ni] (Ln = Gd to Ho) as a function of the atomic number, Z. The J_{Ln-Cu} values are cited from ref 10c. (b) Plot of the cell volume in [Ln_2Ni] as a function of Z.

found to be ca. 16.5μ_B (1.7 K, 5 T) and ca. 15μ_B (1.5 K, 6 T), implying that the absolute total angular momentum, $|J_{Ln}^z|$, is at least 5 (g_J = $^3/_2$) and 6 (g_J = $^5/_4$), respectively. Similar results were obtained for the corresponding Cu analogues.[10c]

To determine the magnetic parameters in detail, we utilize the HF-EPR method. As a reference compound, HF-EPR spectra of polycrystalline [Y_2Ni] were recorded at 4.2 K in a wide range of 90–370 GHz (Figure S3), where the yttrium(III) ion is diamagnetic. We observed a typical powder pattern of the EPR absorption of genuine Ni^{2+} (S = 1). By fitting to the anisotropic S = 1 model (defined as $D_{Ni}\{S_z^2 - (^1/_3)\ S(S+1)\} + E_{Ni}(S_x^2 - S_y^2)$), the optimized parameters were as follows: D_{Ni}/k_B = −3.63(4) K, E_{Ni}/k_B = +0.49(2) K, and g = 2.036(4). The signs of the zero-field splitting (ZFS) parameters were determined by the temperature dependence of the allowed signals.

We measured HF-EPR spectra on polycrystalline [Ho_2Ni] (Figure 2a) in which the transverse-field pattern of the Ni ion appeared just like the results on [Dy_2Ni]. Compared with the spectra of [Y_2Ni], the allowed transition $g \approx 2$ lines are shifted to a lower field. In addition, we found at least two forbidden $g \approx 4$ lines in the almost half field of the allowed band. A large g-value (>11) line was observed on [Ho_2Ni]. The band can be reproduced by $\Delta m_J = \pm 12$ with g_{Ho} = $^5/_4$ being assigned to the forbidden transition between the state of J_{Ho}^z = −6 and 6. The result agrees with the $|J_{Ho}^z|$ value estimated by the pulsed-field magnetization.

HF-EPR spectra of [Tb_2Ni] (Figure 2b) show relatively weak absorptions and randomly oriented powder pattern characteristics like [Y_2Ni], in contrast to those of [Dy_2Ni] and [Ho_2Ni]. We found that all lines shifted to a lower field than those of [Y_2Ni] by ca. 2 T, indicating the distinct presence of a

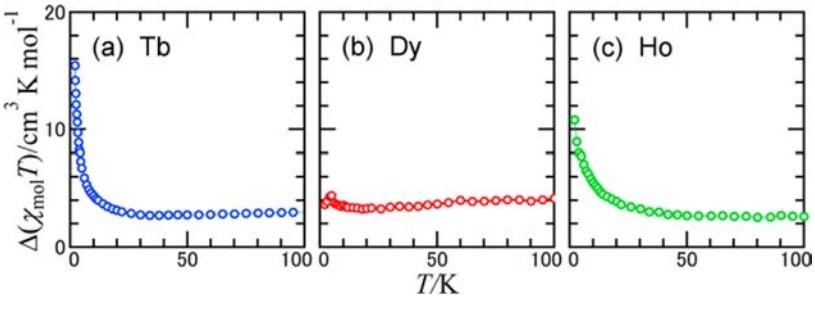

Figure 4. Temperature dependence of the $\chi_{mol}T$ difference, $\Delta(\chi_{mol}T) = (\chi_{mol}T)_{[Ln_2Ni]} - (\chi_{mol}T)_{[Ln_2Pd]}$, for Ln = (a) Tb, (b) Dy, and (c) Ho.

dx.doi.org/10.1021/ic402417h | Inorg. Chem. 2013, 52, 13351–13355

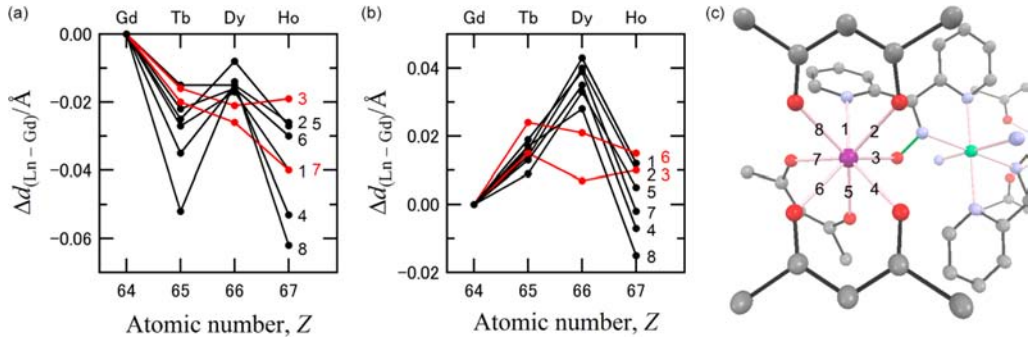

Figure 6. Differences $[\Delta d_{(\text{Ln-Gd})} = (d_{\text{Ln-O}} - d_{\text{Gd-O}})$ or $(d_{\text{Ln-N}} - d_{\text{Gd-N}})]$ of the coordination bond lengths ($d_{\text{Ln-O}}$ and $d_{\text{Ln-N}}$) around the Ln ion on the basis of the Gd analogue for (a) $[Ln_2Ni]$ and (b) $[Ln_2Cu]$. Red lines indicate the anomaly of Ln dependence compared with that of cell volumes (Figure 5b). (c) Selected molecular structure highlighting the geometry around a Ln ion. The coordination bonds and the N−O(oximate) bond are drawn in pink and green, respectively. The 1−8 coordination bonds correspond to the plots numbered in panels a and b.

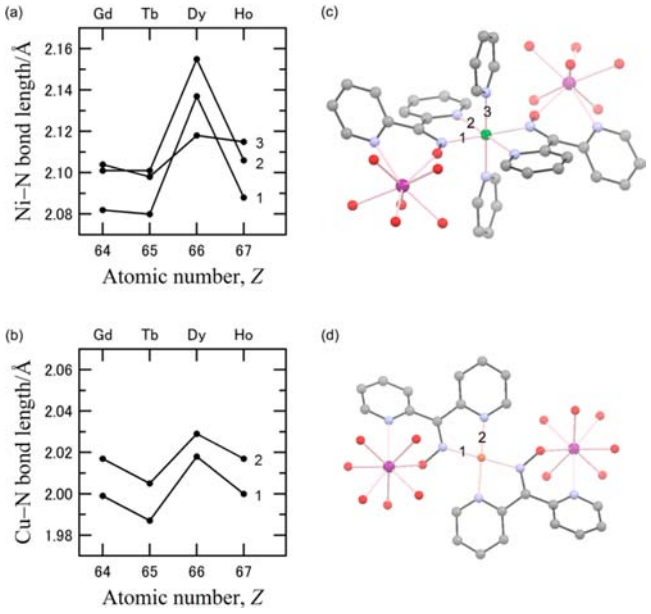

Figure 7. Ln dependence of the coordination bond lengths, (a) $d_{\text{Ni-N}}$ and (b) $d_{\text{Cu-N}}$, for $[Ln_2Ni]$ and $[Ln_2Cu]$, respectively. Selected portions of the molecular structures on (c) $[Ln_2Ni]$ and (d) $[Ln_2Cu]$ are shown. The coordination bonds are highlighted in pink. The numbers labeled on the coordination bonds in panels c and d correspond to those on the plots in panels a and b, respectively.

ferromagnetic bias field (see below). No appreciable Tb signal was observed.

Ferromagnetic Ho−Ni and Tb−Ni couplings were evaluated as follows. The EPR experiments were performed at sufficiently low temperatures so that we can regard Ln ions as Ising spins. This means that the full Hamiltonian of the system can be reduced to an effective Hamiltonian (eq 1) in which the J_{Ln}^{z} value is fixed to that of the ground state. Here, the exchange coupling term is an originally isotropic Heisenberg-type formula; however, the resultant energy levels are those of the Ising model.

$$\hat{H} = -J_{\text{Ho-Ni}}(\hat{J}_{\text{Ho1}}^{z}\hat{S}_{\text{Ni}} + \hat{J}_{\text{Ho2}}^{z}\hat{S}_{\text{Ni}}) + D_{\text{Ni}}\left(S_{\text{Ni}}^{z'^2} - \frac{1}{3}S_{\text{Ni}}(S_{\text{Ni}}+1)\right) + E_{\text{Ni}}(S_{\text{Ni}}^{x'^2} - S_{\text{Ni}}^{y'^2}) + \mu_{\text{B}}H^{z}(g_{\text{Ho}}J_{\text{Ho1}}^{z} + g_{\text{Ho}}J_{\text{Ho2}}^{z}) + \mu_{\text{B}}g_{\text{Ni}}S_{\text{Ni}}H \quad (1)$$

Here, we defined the principal axes of Ln^{3+} as x (first easy axis), y (second easy axis), and z (hard axis). The principal axes of Ni^{2+} are defined as x', y', and z'. The direction of the external field can be assumed to be practically parallel to the easy axis ($H//z$) of magnetization on the Ln ion owing to a field-alignment effect. The method was originally developed for systems with the $S = {}^1/_2$ transition-metal ion (M; Cu^{2+}, etc.), and the same logic holds for the systems with $S = 1$ M ion (Ni^{2+}, etc.). The exchange coupling causes the internal field at the Ni site from adjacent Ln moments, and the Zeeman lines are biased by the exchange field. The frequency-field plot shows the same bias. Negative and positive shifts imply the presence of ferro- and antiferromagnetic couplings between Ln and Ni, respectively. For simplicity, the exchange term is approximated by the exchange bias field in the fitting. The dipolar interactions[14] are disregarded. The perturbation is justified in strong magnetic fields.

Eventually, the following parameters were precisely determined: $J_{\text{Ho-Ni}}/k_{\text{B}} = +0.122(3)$, $D_{\text{Ni}}/k_{\text{B}} = +3.73(8)$, $E_{\text{Ni}}/k_{\text{B}} = -0.70(3)$ K, and $g_{\text{Ni}} = 2.03(7)$ for $[Ho_2Ni]$; $J_{\text{Tb-Ni}}/k_{\text{B}} = +0.216(12)$, $D_{\text{Ni}}/k_{\text{B}} = +4.5(2)$, $E_{\text{Ni}}/k_{\text{B}} = -0.58(6)$ K, and $g = 2.07(4)$ for $[Tb_2Ni]$. By analogy, we determined the sign of D_{Ni} and E_{Ni} in comparison with those of $[Dy_2Ni]$[10a] and $[Y_2Ni]$. The sign of the exchange coupling can be also successfully judged from the relative intensity of three forbidden lines with $g \approx 4$. In the case of $[Ho_2Ni]$, the peak of the lowest field among the forbidden lines was intense, which is an inverse tendency compared with the results on $[Dy_2Ni]$ where the stronger band appears in the higher field because of the antiferromagnetic $J_{\text{Dy-Ni}}$.[10a,b] Thus, we confirm that $J_{\text{Ho-Ni}}$ is ferromagnetic.

Ferromagnetic Gd−Ni coupling was easily characterized as follows. Because of the spin-only nature of Gd^{3+} in $[Gd_2Ni]$, the $g = 2$ line with no bias field was observed because of the $\Delta m_S = \pm 1$ transition within a whole-molecule high-spin state ($S_{\text{total}} = 8$, see below), as was shown by $[GdCu_2]$[11] and [GdM] (M = V and Cu).[6] Alternatively, we measured variable-temperature magnetic susceptibility on a SQUID (Figure 3a) in 500 Oe. The $\chi_{\text{mol}}T$ value monotonically increased on cooling, indicating the ground-state ferromagnetic character of $[Gd_2Ni]$, similar to some other Gd−Ni complexes.[15] The $J_{\text{Gd-Ni}}$ in $[Gd_2Ni]$ was determined according to the van Vleck equation involving Heisenberg spins, giving $J_{\text{Gd-Ni}}/k_{\text{B}} = +0.602(8)$ K with $g_{\text{avg}} = 1.968(3)$. The M_S at 1.8 K and 7 T are $16\mu_{\text{B}}$, supporting the ferromagnetic ground state with $S_{\text{total}} = 8$ (Figure 3b).

dx.doi.org/10.1021/ic402417h | Inorg. Chem. 2013, 52, 13351−13355

In addition to the HF-EPR measurements, we verified the sign of J_{Ln-Ni} by means of the conventional method using the $\chi_{mol}T$ difference, $\Delta(\chi_{mol}T)$, between the Ln−Ni sample and its reference compound involving diamagnetic Pd^{2+} in place of Ni^{2+} (Figure 4). The upsurge of $\Delta(\chi_{mol}T)$ on cooling down to around 2 K for $[Ln_2Ni]$ (Ln = Tb, Dy, and Ho) approximately correspond to the magnitude of J_{4f-3d}. We can characterize $[Dy_2Ni]$ as being almost paramagnetic with a small J_{Dy-Ni} value, whereas both $[Tb_2Ni]$ and $[Ho_2Ni]$ are apparently ferromagnetic. The results are consistent with the HF-EPR study. Note that $\Delta(\chi_{mol}T)$ hardly gives information about the magnitude of J_{Ln-M}, whereas the present HF-EPR method is highly quantitative.

The present results on all of the isomorphous $[Ln_2Ni]$ series are summarized in Figure 5a. The J_{Ln-M} are ferromagnetic, except for Ln = Dy. A similar anomaly has been found at Ln = Dy in the $[Ln_2Cu]$ series.[10c] According to Kahn's model,[16] when the number of 4f electrons is more than seven, the orbital and spin momenta of Ln are parallel ($J = L + S$). The sign of the coupling parameters in the heavy Ln series should be the same as that of the Gd derivative. Thus, the Dy derivatives violate such a general trend.[6,8−11]

Interestingly, we have also found the anomaly of the cell volumes of the Dy derivatives in the crystallographic study (Figure 5b). The volumes of $[Dy_2Ni]$ and $[Dy_2Cu]$ are larger than those of the Gd and Tb derivatives, in contrast to the lanthanide contraction.[17] Investigating the coordination bond lengths, we found short $Dy-O_{oxime}$ and long $M-N_{oxime}$ on both $[Dy_2Ni]$ and $[Dy_2Cu]$ in comparison with their Tb and Ho analogues (Figures 6 and 7). The change of the coordination distances affects crystal fields around the metal ions as well as orbital overlaps between the oxime ligand and a metal ion. Thus, we can conclude that the superexchange predominantly takes place through the oxime bridge. The electron transfer from a 3d(M) orbital to an empty 5d(Ln) orbital is important to ferromagnetic coupling,[16] whereas the electron transfer between 3d(M) and 4f(Ln) orbitals contributes a small, but not negligible, antiferromagnetic coupling.[18] The distorted bridge geometry found in the Dy analogues may reduce the former and gain the latter, giving rise to the observation of antiferromagnetic couplings dominant in the Dy analogues.

CONCLUSIONS

In summary, we demonstrated how to determine quantitatively the 4f−3d exchange couplings for the complexes containing a Ni ion by means of combined HF-EPR and magnetization techniques. The present method is very versatile to determine J_{4f-3d} for general complexes with 3d ions of $S \geq {}^1/_2$. In this case, the ZFS parameters should be taken into account, which may complicate the EPR spectra. However, the high resolution of HF-EPR technique enables us to estimate precise J_{4f-3d} as well as D_{3d} and E_{3d} at the same time.

ASSOCIATED CONTENT

Supporting Information

CIF files; ORTEP drawings for $[Y_2Ni]$, $[Gd_2Ni]$, and $[Ho_2Ni]$; pulsed-field magnetization curve of $[Tb_2Ni]$ at 1.7 K and $[Ho_2Ni]$ at 1.5 K; EPR spectra measured at 4.2 K as a function of frequency for $[Y_2Ni]$; frequency-field diagram for randomly oriented polycrystalline samples of $[Y_2Ni]$; and temperature dependence of EPR spectra at 190 GHz for $[Y_2Ni]$. This material is available free of charge via the Internet at http://pubs.acs.org.

AUTHOR INFORMATION

Corresponding Author

*E-mail: ishi@pc.uec.ac.jp.

Notes

The authors declare no competing financial interest.

ACKNOWLEDGMENTS

This work was partly supported by KAKENHI (grant nos. JSPS/22350059, MEXT/23110711, and JSPS/23750056). H.N. is supported by Innovative Areas − Coordination Programming (2107) from MEXT.

REFERENCES

(1) (a) Kahn, O. *Molecular Magnetism*; VCH: New York, 1993. (b) *Magnetism: Molecules to Materials*; Miller, J. S., Drillon, D., Eds.; Wiley-VCH: Weinheim, Germany, 1999−2005; Vols. *I*−*V*.

(2) Bencini, A.; Benelli, C.; Caneschi, A.; Carlin, R. L.; Dei, A.; Gatteschi, D. *J. Am. Chem. Soc.* **1985**, *107*, 8128.

(3) (a) Osa, S.; Kido, T.; Matsumoto, N.; Re, N.; Pochaba, A.; Mrozinski, J. *J. Am. Chem. Soc.* **2004**, *126*, 420. (b) Mori, F.; Nyui, T.; Ishida, T.; Nogami, T.; Choi, K.-Y.; Nojiri, H. *J. Am. Chem. Soc.* **2006**, *128*, 1440. (c) Pointillart, F.; Bernot, K.; Sessoli, R.; Gatteschi, D. *Chem.—Eur. J.* **2007**, *13*, 1602.

(4) Ishikawa, N.; Sugita, M.; Ishikawa, T.; Koshihara, S.-y.; Kaizu, Y. *J. Am. Chem. Soc.* **2003**, *125*, 8694.

(5) Sessoli, R. *Angew. Chem., Int. Ed.* **2012**, *51*, 43.

(6) (a) Ishida, T.; Watanabe, R.; Fujiwara, K.; Okazawa, A.; Kojima, N.; Tanaka, G.; Yoshii, S.; Nojiri, H. *Dalton Trans.* **2012**, *41*, 13609. (b) Watanabe, R.; Fujiwara, K.; Okazawa, A.; Tanaka, G.; Yoshii, S.; Nojiri, H.; Ishida, T. *Chem. Commun.* **2011**, *47*, 2110.

(7) (a) Nojiri, H.; Ajiro, Y.; Asano, T.; Boucher, J.-P. *New J. Phys.* **2006**, *8*, 218. (b) Nojiri, H.; Choi, K.-Y.; Kitamura, N. *J. Magn. Magn. Mater.* **2007**, *310*, 1468.

(8) (a) Okazawa, A.; Nogami, T.; Nojiri, H.; Ishida, T. *Chem. Mater.* **2008**, *20*, 3110. (b) Okazawa, A.; Fujiwara, K.; Watanabe, R.; Kojima, N.; Yoshii, S.; Nojiri, H.; Ishida, T. *Polyhedron* **2011**, *30*, 3121.

(9) (a) Ueki, S.; Ishida, T.; Nogami, T.; Choi, K.-Y.; Nojiri, H. *Chem. Phys. Lett.* **2007**, *440*, 263. (b) Fujiwara, K.; Okazawa, A.; Tanaka, G.; Yoshii, S.; Nojiri, H.; Ishida, T. *Chem. Phys. Lett.* **2012**, *530*, 49.

(10) (a) Okazawa, A.; Nogami, T.; Nojiri, H.; Ishida, T. *Inorg. Chem.* **2008**, *47*, 9763. (b) Okazawa, A.; Nogami, T.; Nojiri, H.; Ishida, T. *Inorg. Chem.* **2009**, *48*, 3292. (c) Okazawa, A.; Watanabe, R.; Nezu, M.; Shimada, T.; Yoshii, S.; Nojiri, H.; Ishida, T. *Chem. Lett.* **2010**, *39*, 1331.

(11) Shimada, T.; Okazawa, A.; Kojima, N.; Yoshii, S.; Nojiri, H.; Ishida, T. *Inorg. Chem.* **2011**, *50*, 10555.

(12) Mori, F.; Ishida, T.; Nogami, T. *Polyhedron* **2005**, *24*, 2588.

(13) Okazawa, A.; Nojiri, H.; Ishida, T.; Kojima, N. *Polyhedron* **2011**, *30*, 3140.

(14) For $[Ho_2Ni]$, a dipolar interaction is estimated to be at most 0.024 K for $[Ho_2Ni]$ ($g_{Ho} = {}^5/_4$, $g_{Ni} = 2$, $r_{Ho-Ni} = 5.099$ Å; $J_{Ho-Ni} = 2\mu_B{}^2\mu_0 g_{Ln} g_{Ni}/4\pi r_{Ho-Ni}{}^3$).

(15) (a) Costes, J.-P.; Dahan, F.; Dupuis, A.; Laurent, J.-P. *Inorg. Chem.* **1997**, *36*, 4284. (b) Igarashi, S.; Kawaguchi, S.; Yukawa, Y.; Tuna, F.; Winpenny, R. *Dalton Trans.* **2009**, 3140.

(16) Andruh, M.; Ramade, I.; Codjovi, E.; Guillou, O.; Kahn, O.; Trombe, J. C. *J. Am. Chem. Soc.* **1993**, *115*, 1822.

(17) Huheey, J. E.; Keiter, E. A.; Keiter, R. L. *Inorganic Chemistry: Principles of Structure and Reactivity*; HarperCollins: New York, 1993.

(18) Costes, J.-P.; Dahan, F.; Dupuis, A.; Laurent, J.-P. *Inorg. Chem.* **2000**, *39*, 169.